Computing resonance positions, widths, and cross sections via the Feshbach-Fano *R*-matrix method: Application to potential scattering

Přemysl Kolorenč,[1] Vincent Brems,[2] and Jiří Horáček[1]
[1]*Institute of Theoretical Physics, Faculty of Mathematics and Physics, Charles University in Prague, Czech Republic*
[2]*Department of Chemical Physics, J. Heyrovský Institute of Physical Chemistry, Dolejškova 3, 18223 Praha 8, Czech Republic*
(Received 23 February 2005; published 13 July 2005)

The general Feshbach-Fano *R*-matrix procedure proposed recently by Nestmann [J. Phys. B **31**, 3929 (1998)] makes it possible to construct resonance metastable states of transient molecular ions and their coupling elements to the background scattering continuum. These quantities are needed for the study of nuclear dynamics in the framework of the nonlocal resonance model. The performance of this approach is carefully studied and its properties analyzed in the field of potential scattering. An improvement of the Nestmann procedure which makes the calculation more stable and robust is proposed.

DOI: 10.1103/PhysRevA.72.012708 PACS number(s): 03.65.Nk, 34.10.+x, 34.50.−s, 34.80.−i

I. INTRODUCTION

Resonances are one of the most striking and ubiquitous phenomena in scattering experiments (e.g., in nuclear, atomic, or molecular physics, physical chemistry, as well as in the physics of conductors or semiconductors, quantum dots, or Bose-Einstein condensates; see Refs. [1–5], and references therein). They appear as pronounced structures of spectra in energy-resolved experiments and are associated with a time delay of the fragmentation process in time-resolved experiments. Mathematically, they are associated with poles, $z_{res}=\epsilon_{res}-i\Gamma_{res}/2$, of the scattering *S*-matrix in the complex-energy plane. ϵ_{res} and Γ_{res} are called the position and width of the resonance. In practice, determining z_{res} is usually a difficult numerical task (for which different methods are available like Stieltjes imaging [6], stabilization method [7], shooting methods [8], complex scaling [9], complex absorbing potential [3], etc.). Resonances are associated with the resonance component of the cross section. The celebrated Breit-Wigner formula [10],

$$\sigma_{res}=\frac{1}{\pi}\frac{\Gamma_{res}^2}{(\epsilon-\epsilon_{res})^2+\Gamma_{res}^2/4},$$

can usually be fitted to the resonance component of the cross section. This formula is of course not valid in the vicinity of fragmentation threshold or in the case of overlapping resonances. It has been generalized by Kapur and Peierls [11], Wigner and Eisenbud [12]; Fano [13], and Feshbach [14,15], introducing energy-dependent parameters $\epsilon_{res}(\epsilon)\equiv\epsilon_d+\Delta(\epsilon)$ and $\Gamma_{res}(\epsilon)\equiv\Gamma(\epsilon)$ [ϵ_d is the discrete-state energy, $\Delta(\epsilon)$ is the energy-dependent level shift, and $\Gamma(\epsilon)$ is the energy-dependent width]. The poles of the *S*-matrix can be found as a solution of implicit equation,

$$\epsilon_d+\Delta(z_{res})-\frac{i}{2}\Gamma(z_{res})-z_{res}=0. \quad (1)$$

Every solution of this equation corresponds to a pole of the *S*-matrix but may not represent any experimentally observable resonant phenomenon. The Feshbach-Fano (FF) method allows us to associate square integrable wave functions, within a physically relevant linear functional space $\mathcal{Q}$, with the resonances. This approach permits us to determine the physically relevant resonances only, their corresponding wave functions and cross sections. Once the subspace $\mathcal{Q}$ is determined on the basis of the particular physical context, the FF method provides a detailed and intuitive understanding of the resonant process (for recent comprehensive discussion, see Refs. [16–19]). The basic idea of the Feshbach-Fano *R*-matrix (FFR) method introduced in Nestmann's seminal article [20] is to define $\mathcal{Q}$ as a subset of the scattering states fulfilling the Wigner-Eisenbud boundary conditions on the surface of the *R*-matrix sphere complemented with a set of additional particular conditions.

The major reason why we consider the FFR method is its capability to construct necessary potentials and coupling elements to be used in the application of the nonlocal resonance model (NRM) to electron-molecule scattering. NRM is based on the assumption that a temporary molecular negative-ion state (resonance) is formed in the process of the collision and that this resonance accounts for the coupling of the electronic scattering dynamics with the nuclear motion (see Ref. [21] for a comprehensive review). The nonlocal resonance theory yields cross sections for vibrational excitation (VE), dissociative electron attachment (DEA), as well as associative electron detachment (AED) in very good agreement with experimental data describing all the complexity of the problem, i.e., the theory reproduced successfully threshold peaks in VE, Wigner cusps in the process of DEA, isotope effect in DEA, etc. The theory predicted even other interesting features—oscillations in VE cross sections below the opening of the DEA channel—the existence of which was confirmed subsequently by experiment [22].

In NRM the resonance is represented by a square-integrable discrete state $|\varphi_d\rangle$—spanning the $\mathcal{Q}$ space—which interacts with a continuum of background scattering states $|^{bg}\varphi_\epsilon\rangle$—spanning the complementary space $\mathcal{P}$—via coupling matrix elements $V_{d\epsilon}$. The discrete state-continuum coupling term $V_{d\epsilon}$ is related to the energy-dependent width via $\Gamma(\epsilon)=2\pi|V_{d\epsilon}|^2$. Once the discrete state $|\varphi_d\rangle$ and the coupling $V_{d\epsilon}$ are known the cross sections can be very efficiently calculated (see Ref. [23], and references therein). The construction

of the discrete state is, however, complicated and the calculation of the coupling $V_{d\epsilon}$ from first principles is a very difficult task. Several methods of determining the energy-dependent resonance widths associated with resonance states have been discussed recently by Sommerfeld and Meyer [24]. The FFR method [20] makes it possible to extract from the R-matrix results the discrete state, its potential curve, the background phase shift, and the corresponding coupling terms with the electronic continuum. The connection between the R-matrix theory and the FF formalism was discussed by Feshbach [15] and more recently by Kazansky [25] and Rotter [26]. In order to apply the FFR formalism to electron-molecule scattering, Nestmann [20] developed an approximation of practical importance. This approximation was applied to several molecules at the equilibrium geometry of the ground state (N_2, C_3H_6, N_2O). In addition this approach was later applied successfully by Beyer *et al.* to study the DEA spectrum of CF_3Cl [27–29], by Brems *et al.* to study a long-standing problem—the problem of DEA and VE of the fluorine molecule [30]. More recently Nestmann *et al.* applied the FFR methodology to the DEA spectrum of ozone [31,32]. Calculations of this type are a very complex task involving several approximations the role of which has not been controlled and studied in detail.

The purpose of this paper is twofold: first, to test Nestmann's method on clearly defined cases, i.e., to use well-known potentials in one dimension which support several resonance states and which have been studied by other authors, and to establish the limits of the FFR method; second, to propose an improvement of the Nestmann's approximation which makes the calculation more stable and more robust. The paper is organized as follows: In Sec. II, a brief overview of the projection-operator approach and R-matrix theory is given, followed by detailed derivation of the FFR method. In particular, in Secs. II C and II D, two substantial improvements to Nestmann's FFR are proposed. In Sec. III the method is applied to two qualitatively different potential scattering problems and the results are carefully analyzed. The paper is summarized in Sec. IV.

II. THEORY

A. Projection-operator approach

In this section we give a brief outline of the projection-operator formalism [13–15] as applied to resonant potential scattering. A more detailed description can be found in Ref. [33]. The main idea of the approach is to divide the whole Hilbert space into two subspaces, $\mathcal{H}=\mathcal{Q}\oplus\mathcal{P}$. The resonant part $\mathcal{Q}$ corresponds to all rapid variations of the scattering phase shifts and cross sections, while the scattering corresponding to the remaining part $\mathcal{P}$ (background scattering) is expected to produce only smooth and slowly varying phase shifts in the energy interval of interest and can be therefore treated using different approximations.

The separation is done by introducing the projection operators P and Q,

$$P^2=P,\quad Q^2=Q,\quad P+Q=1,\quad PQ=QP=0. \tag{2}$$

For energy near resonance the wave function can be described by a square integrable function since the amplitude of the oscillatory tail is expected to be much smaller than the values of the wave function in the interaction region. This suggests the choice of the projector Q in the form

$$Q=\sum_{n=1}^{N_d}|\varphi_{d,n}\rangle\langle\varphi_{d,n}|, \tag{3}$$

where the $\varphi_{d,n}(r)$ are square integrable functions (often called discrete states). The separation of the Hilbert space into the resonant and nonresonant parts leads to corresponding separation of the T-matrix, $T=T_{res}+T_{bg}$.

In case of a spherically symmetric scattering potential the P component of the scattering wave function at energy ϵ can be obtained as follows. By projections of the Schrödinger equation $(H-\epsilon)|\Psi_\epsilon^{(\pm)}\rangle=0$ we get a system of coupled equations

$$(\epsilon-H_{PP})P|\Psi_\epsilon^{(\pm)}\rangle=H_{PQ}Q|\Psi_\epsilon^{(\pm)}\rangle, \tag{4}$$

$$(\epsilon-H_{QQ})Q|\Psi_\epsilon^{(\pm)}\rangle=H_{QP}P|\Psi_\epsilon^{(\pm)}\rangle \tag{5}$$

(we have used the abbreviation H_{QP} for QHP, etc.) for each partial wave component (we omit the indexes l,m) of the scattering wave function. This system can be resolved with respect to the P component, yielding the Schrödinger equation

$$\tilde{H}_\epsilon P|\Psi_\epsilon^{(\pm)}\rangle=\epsilon P|\Psi_\epsilon^{(\pm)}\rangle \tag{6}$$

with the optical-potential Hamiltonian

$$\tilde{H}_\epsilon=H_{PP}+H_{PQ}(\epsilon-H_{QQ})^{-1}H_{QP}. \tag{7}$$

The resonant scattering T-matrix

$$T_{res}(\epsilon',\epsilon)=\langle{}^{bg}\varphi_{\epsilon'}^{(-)}|H-H_{PP}|\Psi_\epsilon^{(+)}\rangle \tag{8}$$

can be written in terms of the background solutions $|{}^{bg}\varphi_\epsilon^{(\pm)}\rangle$ (energy normalized eigenfunctions of H_{PP}) as

$$T_{res}(\epsilon',\epsilon)=\langle{}^{bg}\varphi_{\epsilon'}^{(-)}|H_{PQ}[\epsilon-H_{QQ}-H_{QP}(\epsilon-H_{PP}+i\varepsilon)^{-1}H_{PQ}]^{-1}H_{QP}|{}^{bg}\varphi_\epsilon^{(+)}\rangle. \tag{9}$$

The poles of the T-matrix are then determined by the equation

$$\det[z_{res}-H_{QQ}-H_{QP}(z_{res}-H_{PP}+i\varepsilon)^{-1}H_{PQ}]=0. \tag{10}$$

Equation (1) is the special case of this equation for isolated resonance.

In the case of isolated resonance ($Q=|\varphi_d\rangle\langle\varphi_d|$) the generalized Breit-Wigner formula for the resonant part of the T-matrix can be derived [13,14]. Let us define the discrete state energy

$$\epsilon_d=\langle\varphi_d|H|\varphi_d\rangle \tag{11}$$

and the complex level-shift function

$$F(\epsilon)=\langle\varphi_d|H_{QP}(\epsilon-H_{PP}+i\varepsilon)^{-1}H_{PQ}|\varphi_d\rangle. \tag{12}$$

Using the spectral representation of the Green's function $(\epsilon-H_{PP}+i\varepsilon)^{-1}$ the level shift can be expressed in terms of the discrete state-continuum coupling matrix elements

$$V_{d\epsilon} = \langle \varphi_d | H |^{bg} \varphi_\epsilon^{(+)} \rangle \tag{13}$$

as

$$F(\epsilon) = \Delta(\epsilon) - \frac{i}{2}\Gamma(\epsilon), \tag{14}$$

$$\Gamma(\epsilon) = 2\pi |V_{d\epsilon}|^2, \tag{15}$$

$$\Delta(\epsilon) = \frac{1}{2\pi} \mathrm{P} \int \frac{\Gamma(\epsilon')}{\epsilon - \epsilon'} d\epsilon'. \tag{16}$$

The resonant part of the T-matrix is then given by

$$T_{res}(\epsilon) = \frac{1}{2\pi} \frac{\Gamma(\epsilon)}{\epsilon - \epsilon_d - \Delta(\epsilon) + \frac{i}{2}\Gamma(\epsilon)}. \tag{17}$$

B. *R*-matrix theory

The key idea of the R-matrix theory [12,34] is to divide the whole space into two regions by a sphere Ω centered on the target. The radius r_Ω of the sphere is chosen so that outside of the sphere (external region) the interaction can be approximated by an effective single-particle potential (usually a multipole expansion). In the particular case of spherically symmetric potential scattering r_Ω is chosen so that the interaction potential vanishes outside the sphere and the wave function can be expressed by means of spherical Bessel functions in the external region. The modified Hamiltonian

$$H^\Omega(r) = H(r) + L(r) = H(r) + \frac{1}{2}\delta(r - r_\Omega)\frac{d}{dr}, \tag{18}$$

symmetric in the space of functions defined in the internal region $\langle 0, r_\Omega \rangle$ and satisfying the condition $\varphi(0)=0$, is introduced. It provides discretization of the scattering continuum via solving the eigenvalue problem inside Ω,

$$H^\Omega(r)\varphi_k^\Omega(r) = E_k^\Omega \varphi_k^\Omega(r), \tag{19}$$

with $\varphi_k^\Omega(r)$ normalized to unity within the interval $\langle 0, r_\Omega \rangle$. The quantity

$$R(\epsilon) = \frac{1}{2}\sum_k \frac{[\varphi_k^\Omega(r_\Omega)]^2}{E_k^\Omega - \epsilon} \tag{20}$$

is the one-dimensional analog of the R-matrix and has the simple meaning of the inverse logarithmic derivative of the solution of the Schrödinger equation at r_Ω. It therefore provides the boundary condition for the solution in the external region,

$$\Psi_\epsilon^{(\pm)}(r_\Omega) = R(\epsilon) \left. \frac{d}{dr}\Psi_\epsilon^{(\pm)}(r) \right|_{r=r_\Omega}. \tag{21}$$

Within the internal region the solution can then be expanded in terms of the R-matrix basis $\{\varphi_k^\Omega(r)\}$ as

$$\Psi_\epsilon^{(\pm)}(r) = \frac{1}{2}\sum_k \varphi_k^\Omega(r) \frac{\varphi_k^\Omega(r_\Omega)}{E_k^\Omega - \epsilon} \left. \left(\frac{d}{dr}\Psi_\epsilon^{(\pm)}(r) \right) \right|_{r=r_\Omega}. \tag{22}$$

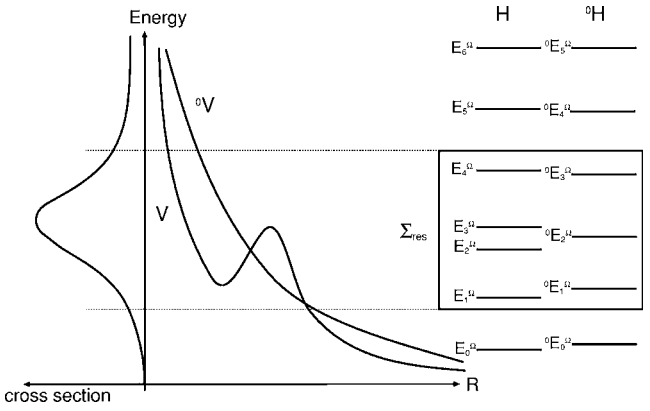

FIG. 1. Comparison of the R-matrix spectra of resonant and nonresonant systems.

C. Feshbach-Fano *R*-matrix (FFR) method

In this section we show how the results of the R-matrix theory can be used for definition of the discrete state $|\varphi_d\rangle$ and related quantities ϵ_d, $\Gamma(\epsilon)$ and $\Delta(\epsilon)$. The general multichannel form of the FFR method was described elsewhere [20], so we give here only the simple formulas, suitable for one-dimensional potential scattering.

Let the scattering phase shift show a resonance structure in a certain energy region Σ_{res}, see Fig. 1. Assuming that the radius r_Ω of the sphere Ω is chosen to be sufficiently large, the square integrable discrete state wave function $\varphi_d(r)$ associated with the resonance can be considered to be completely contained inside the R-matrix region. Under this assumption it can be expanded in terms of the R-matrix basis (19) as

$$\varphi_d(r) = \sum_{E_k^\Omega \in \Sigma_{res}} c_k^\Omega \varphi_k^\Omega(r) \tag{23}$$

provided Σ_{res} is chosen such that it covers all the spectral domain where the discrete state is expected to interact with the background continuum. In order to ensure that $\varphi_d(r)$ [Eq. (23)] is integrable on $\langle 0, \infty \rangle$ it has to be set to constant zero outside the R-matrix sphere. Only the condition

$$\varphi_d(r_\Omega) = 0 \tag{24}$$

has to be satisfied. The second required condition of vanishing first derivative of the wave function,

$$\left. \frac{d\varphi_d(r)}{dr} \right|_{r=r_\Omega} = 0, \tag{25}$$

is met automatically because of the following reasons. It can be shown that in case that complete basis is used for solving the problem (19) then for all k the derivatives of $\varphi_k^\Omega(r)$ vanish at r_Ω. Because there is only a finite number of terms included in the expansion (23) Eq. (25) follows immediately.

Let the energy interval Σ_{res} contain N levels E_k^Ω. Except the case $N=2$ the condition (24) does not determine the discrete state completely. Some criterion defining a resonance is needed. It can be found by comparison with a similar system possessing no resonance in the region Σ_{res}. We have to con-

struct such a model Hamiltonian $^{\circ}H$ for which the phase shift is close to what we expect to be the background phase shift for the full problem H. The comparison is implemented through the R-matrix spectrum obtained by solving the eigenvalue problem similar to Eq. (19),

$$^{\circ}H^{\Omega}(r)\ {}^{\circ}\varphi_k^{\Omega}(r) = {}^{\circ}E_k^{\Omega}\ {}^{\circ}\varphi_k^{\Omega}(r). \tag{26}$$

In the case of single isolated resonance it has been shown in some examples [20] that it is possible to choose Σ_{res} such that $^{\circ}N$ (number of eigenvalues $^{\circ}E_k^{\Omega}$ lying in Σ_{res}) is equal to $N-1$. In general, the FFR method defines the number of resonances within Σ_{res} as the difference between the numbers of levels E_k^{Ω} and $^{\circ}E_k^{\Omega}$ contained in this energy region. Typical comparison of the R-matrix spectra of resonant and similar nonresonant systems is schematically plotted in Fig. 1.

The background scattering is characterized by the eigenstates $|^{bg}\varphi_j^{\Omega}\rangle$ of the projected Hamiltonian $^{bg}H^{\Omega}=PH^{\Omega}P$. The basic assumption of the FFR method is the existence of a unitary mapping,

$$^{bg}\varphi_j^{\Omega}(r) = \sum_{^{\circ}E_k^{\Omega}\in\Sigma_{res}} a_{jk}\ {}^{\circ}\varphi_k^{\Omega}(r), \quad \sum_l a_{il}^* a_{jl} = \delta_{ij}, \tag{27}$$

for $^{bg}E_j$ from Σ_{res}. In other words, within Σ_{res}, the Hilbert space corresponding to the model system is used as an approximation to the background Hilbert space of the original one. Because we have assumed that the discrete state interacts with the background continuum only within the Σ_{res} domain it is justified to take $^{bg}\varphi^{\Omega}(r)=\varphi^{\Omega}(r)$ for levels lying outside of this energy region—the resonance does not affect the spectrum outside Σ_{res} at all. The projector onto the $\mathcal{P}$ subspace, restricted within the R-matrix sphere, can then be expressed as

$$P^{\Omega} = \sum_{^{\circ}E_k^{\Omega}\in\Sigma_{res}} |{}^{\circ}\varphi_k^{\Omega}\rangle\langle{}^{\circ}\varphi_k^{\Omega}| + \sum_{E_k^{\Omega}\notin\Sigma_{res}} |\varphi_k^{\Omega}\rangle\langle\varphi_k^{\Omega}|. \tag{28}$$

In this representation the condition $P^{\Omega}Q=0$ yields a system of linear equations for the expansion coefficients c_k^{Ω},

$$\sum_{k=1}^{N} c_k^{\Omega}\langle{}^{\circ}\varphi_j^{\Omega}|\varphi_k^{\Omega}\rangle = 0, \quad {}^{\circ}E_j^{\Omega}\in\Sigma_{res}. \tag{29}$$

A slightly different discussion leading to this system can be found in Ref. [30].

Equations (24) and (29) form a homogeneous system of N linear equations for N expansion coefficients c_k^{Ω} (N is the number of levels E_k^{Ω} within the Σ_{res} domain and we are considering the case of single isolated resonance). For existence of the solution it is necessary that the determinant of the system satisfies

$$\begin{vmatrix} \langle{}^{\circ}\varphi_1^{\Omega}|\varphi_1^{\Omega}\rangle & \langle{}^{\circ}\varphi_1^{\Omega}|\varphi_2^{\Omega}\rangle & \cdots & \langle{}^{\circ}\varphi_1^{\Omega}|\varphi_N^{\Omega}\rangle \\ \vdots & & \ddots & \\ \langle{}^{\circ}\varphi_{N-1}^{\Omega}|\varphi_1^{\Omega}\rangle & \langle{}^{\circ}\varphi_{N-1}^{\Omega}|\varphi_2^{\Omega}\rangle & \cdots & \langle{}^{\circ}\varphi_{N-1}^{\Omega}|\varphi_N^{\Omega}\rangle \\ \varphi_1^{\Omega}(r_{\Omega}) & \varphi_2^{\Omega}(r_{\Omega}) & \cdots & \varphi_N^{\Omega}(r_{\Omega}) \end{vmatrix} = 0. \tag{30}$$

In general this is not true for any arbitrary model potential. The condition (30) can be rather understood as a constraint for the Hamiltonian $^{\circ}H$. For realistic problems, however, it is not possible to find $^{\circ}H$ such that the condition (30) is fulfilled. Therefore, because the condition (24) is essential for ensuring the L^2 integrability of φ_d, Eq. (29) can be satisfied only approximately. The most straightforward way is to apply some minimization procedure. In actual calculations [20,27–32], a different approach has been chosen because the overlap integrals $\langle{}^{\circ}\varphi_j^{\Omega}|\varphi_k^{\Omega}\rangle$ are quantities which are not easily extracted from the existing implementation of the *ab initio* R-matrix code.

Following Ref. [20], we will show that it is possible to find an approximation to the overlap integrals such that condition (24) is satisfied when Eq. (29) is solved within this approximation. Under assumption (27), $\varphi_k^{\Omega}(r)$ can be expanded as (for $E_k^{\Omega}\in\Sigma_{res}$)

$$\varphi_k^{\Omega}(r) = \sum_{^{\circ}E_l^{\Omega}\in\Sigma_{res}} d_{kl}\ {}^{\circ}\varphi_l^{\Omega}(r) + c_k\varphi_d(r)$$

$$d_{\mathrm{kl}} = \langle{}^{\circ}\varphi_l^{\Omega}|\varphi_k^{\Omega}\rangle. \tag{31}$$

From the Schrödinger equation projected into the $\mathcal{P}$ space (6) in the Ω-confined form with $\epsilon=E_k^{\Omega}$ we arrive at

$$\left({}^{bg}H^{\Omega} + \frac{PH^{\Omega}|\varphi_d\rangle\langle\varphi_d|H^{\Omega}P}{E_k^{\Omega}-\epsilon_d}\right)P|\varphi_k^{\Omega}\rangle = E_k^{\Omega}P|\varphi_k^{\Omega}\rangle. \tag{32}$$

Introducing the residual potential

$$V_{\mathrm{rsd}} = {}^{bg}H^{\Omega} - {}^{\circ}H^{\Omega} \tag{33}$$

and, multiplying Eq. (32) by $\langle{}^{\circ}\varphi_j^{\Omega}|$ from the left, we obtain

$$\langle{}^{\circ}\varphi_j^{\Omega}|\,{}^{\circ}H^{\Omega}|P\varphi_k^{\Omega}\rangle + \langle{}^{\circ}\varphi_j^{\Omega}|V_{\mathrm{rsd}}|P\varphi_k^{\Omega}\rangle + \frac{\langle{}^{\circ}\varphi_j^{\Omega}|H^{\Omega}|\varphi_d\rangle\langle\varphi_d|H^{\Omega}|P\varphi_k^{\Omega}\rangle}{E_k^{\Omega}-\epsilon_d} = E_k^{\Omega}\langle{}^{\circ}\varphi_j^{\Omega}|P\varphi_k^{\Omega}\rangle. \tag{34}$$

Applying the representation (28) for the P projector yields

$${}^{\circ}E_j^{\Omega}d_{\mathrm{kj}} + \sum_{^{\circ}E_l^{\Omega}\in\Sigma_{res}} d_{\mathrm{kl}}\left(\langle{}^{\circ}\varphi_j^{\Omega}|V_{\mathrm{rsd}}|\,{}^{\circ}\varphi_l^{\Omega}\rangle + \frac{\langle{}^{\circ}\varphi_j^{\Omega}|H^{\Omega}|\varphi_d\rangle\langle\varphi_d|H^{\Omega}|\,{}^{\circ}\varphi_l^{\Omega}\rangle}{E_k^{\Omega}-\epsilon_d}\right) = E_k^{\Omega}d_{\mathrm{kj}}. \tag{35}$$

With the notation

$$v_{\mathrm{kj}} = \sum_{^{\circ}E_l^{\Omega}\in\Sigma_{res}} d_{\mathrm{kl}}\langle{}^{\circ}\varphi_j^{\Omega}|V_{\mathrm{rsd}}|\,{}^{\circ}\varphi_l^{\Omega}\rangle, \tag{36}$$

$$B_k = \sum_{^{\circ}E_l^{\Omega}\in\Sigma_{res}} d_{\mathrm{kl}}\frac{\langle\varphi_d|H^{\Omega}|\,{}^{\circ}\varphi_l^{\Omega}\rangle}{E_k^{\Omega}-\epsilon_d} \tag{37}$$

the resulting formula for the overlap boils down to an implicit equation for d_{kj},

$$d_{\mathrm{kj}} = \langle{}^{\circ}\varphi_j^{\Omega}|\varphi_k^{\Omega}\rangle = \frac{v_{\mathrm{kj}} + \langle{}^{\circ}\varphi_j^{\Omega}|H^{\Omega}|\varphi_d\rangle B_k}{E_k^{\Omega} - {}^{\circ}E_j^{\Omega}}. \tag{38}$$

The only approximation applied so far is the assumption (27). Under the additional presumption that the contributions v_{kj} of the residual potential are small in comparison with the B_k, representing the interaction of $|\varphi_d\rangle$ with the background, we get the proportionality

$$\langle {}^{\circ}\varphi_j^{\Omega}|\varphi_k^{\Omega}\rangle = B_k \frac{\langle {}^{\circ}\varphi_j^{\Omega}|H^{\Omega}|\varphi_d\rangle}{E_k^{\Omega} - {}^{\circ}E_j^{\Omega}} \tag{39}$$

with unknown coefficients B_k and $\langle {}^{\circ}\varphi_j^{\Omega}|H^{\Omega}|\varphi_d\rangle$. The B_k coefficients are approximated in such a way that Eq. (29) gives the discrete state wave function vanishing at r_{Ω}. The latter constraint is equivalent to the statement that the P projector does not affect the amplitudes $\varphi_k^{\Omega}(r_{\Omega})$, more precisely $(P\varphi_k^{\Omega})(r_{\Omega}) = \varphi_k^{\Omega}(r_{\Omega})$. Within Σ_{res}, this can be rewritten using Eq. (28) as

$$\sum_{{}^{\circ}E_j^{\Omega} \in \Sigma_{res}} \langle {}^{\circ}\varphi_j^{\Omega}|\varphi_k^{\Omega}\rangle \, {}^{\circ}\varphi_j^{\Omega}(r_{\Omega}) = \varphi_k^{\Omega}(r_{\Omega}). \tag{40}$$

Applying the approximation (39) we arrive at

$$B_k = \left(\sum_{{}^{\circ}E_l^{\Omega} \in \Sigma_{res}} \frac{\langle {}^{\circ}\varphi_l^{\Omega}|H^{\Omega}|\varphi_d\rangle \, {}^{\circ}\varphi_l^{\Omega}(r_{\Omega})}{E_k^{\Omega} - {}^{\circ}E_l^{\Omega}} \right)^{-1} \varphi_k^{\Omega}(r_{\Omega}). \tag{41}$$

The discrete state wave function can now be constructed in a self-consistent iterative process. As a first approximation of $\varphi_d(r)$ we take the wave function $\varphi_l^{\Omega}(r)$ with corresponding energy E_l^{Ω} that is the closest to the expected discrete state energy,

$$c_k^{\Omega,(1)} = \delta_{\mathrm{lk}}, \quad \epsilon_d^{(1)} = E_l^{\Omega}. \tag{42}$$

Then we have to construct the first approximation to the coupling elements $\langle {}^{\circ}\varphi_l^{\Omega}|H^{\Omega}|\varphi_d\rangle$. To do so we insert $\langle {}^{\circ}\varphi_l^{\Omega}|H^{\Omega}|\varphi_d\rangle = 1$ into (39) and (41) and obtain a zeroth approximation of the overlap integrals,

$$\langle {}^{\circ}\varphi_j^{\Omega}|\varphi_k^{\Omega}\rangle^{(0)} = \left(\sum_{{}^{\circ}E_l^{\Omega} \in \Sigma_{res}} \frac{{}^{\circ}\varphi_l^{\Omega}(r_{\Omega})}{E_k^{\Omega} - {}^{\circ}E_l^{\Omega}} \right)^{-1} \frac{\varphi_k^{\Omega}(r_{\Omega})}{E_k^{\Omega} - {}^{\circ}E_j^{\Omega}}. \tag{43}$$

First approximation of the coupling elements is then given by

$$\langle {}^{\circ}\varphi_j^{\Omega}|H^{\Omega}|\varphi_d\rangle^{(1)} = \sum_{E_k^{\Omega} \in \Sigma_{res}} \delta_{lk} E_k^{\Omega} \langle {}^{\circ}\varphi_j^{\Omega}|\varphi_k^{\Omega}\rangle^{(0)}. \tag{44}$$

The iterations proceed as follows. The couplings $\langle {}^{\circ}\varphi_j^{\Omega}|H^{\Omega}|\varphi_d\rangle^{(i)}$ are inserted into Eqs. (39) and (41) to obtain improved approximation of the overlap integrals $\langle {}^{\circ}\varphi_j^{\Omega}|\varphi_k^{\Omega}\rangle^{(i)}$, which are then used in Eq. (29) to determine the next approximation of the expansion coefficients $\{c_k^{\Omega,(i+1)}\}$. Corresponding approximation of the coupling integrals is obtained from

$$\langle {}^{\circ}\varphi_j^{\Omega}|H^{\Omega}|\varphi_d\rangle^{(i+1)} = \sum_{E_k^{\Omega} \in \Sigma_{res}} c_k^{\Omega,(i+1)} E_k^{\Omega} \langle {}^{\circ}\varphi_j^{\Omega}|\varphi_k^{\Omega}\rangle^{(i)} \tag{45}$$

and used again to improve the overlaps $\langle {}^{\circ}\varphi_j^{\Omega}|\varphi_k^{\Omega}\rangle$ and expansion coefficients.

In the case of single resonance the iterations stop after the first step, because $\{c_k^{\Omega,(2)}\}$ is already a self-consistent solution. In the case of overlapping resonances the set of discrete states have to be orthonormalized in each step by diagonalizing the Hamiltonian in the obtained $\mathcal{Q}$ subspace [see the end of this section and Eq. (51)], which breaks the consistency of the solution. In all studied examples of multiple resonances, however, the iterations always converged very rapidly.

Having defined the discrete state, we can construct the projector $P^{\Omega} = 1^{\Omega} - Q$ and the background spectrum

$$[{}^{bg}H^{\Omega}(r) - {}^{bg}E_l^{\Omega}]{}^{bg}\varphi_l^{\Omega}(r) = 0. \tag{46}$$

If the eigenfunctions are expanded into the $\{\varphi_k^{\Omega}(r)\}$ basis as

$${}^{bg}\varphi_k^{\Omega}(r) = \sum_l b_{\mathrm{kl}}^{\Omega} \varphi_l^{\Omega}(r), \tag{47}$$

a simple formula for the coupling with the discrete state can be found:

$$\langle \varphi_d|H|{}^{bg}\varphi_k^{\Omega}\rangle = \langle \varphi_d|H^{\Omega}|{}^{bg}\varphi_k^{\Omega}\rangle = \sum_{E_l^{\Omega} \in \Sigma_{res}} b_{\mathrm{kl}}^{\Omega} E_l^{\Omega} c_l^{\Omega}. \tag{48}$$

The extension to the continuous energy is done when the background scattering states ${}^{bg}\varphi_{\epsilon}^{(+)}(r)$ are expanded into $\{{}^{bg}\varphi_l^{\Omega}(r)\}$ using the formula (22), arriving at

$$V_{d\epsilon} = \langle \varphi_d|H|{}^{bg}\varphi_{\epsilon}^{(+)}\rangle = \frac{1}{2}\sum_{\mathrm{kl}} b_{\mathrm{kl}}^{\Omega} E_l^{\Omega} c_l^{\Omega} \frac{{}^{bg}\varphi_k^{\Omega}(r_{\Omega})}{{}^{bg}E_k^{\Omega} - \epsilon} \times \left(\frac{d}{dr} {}^{bg}\varphi_{\epsilon}^{(+)}(r) \right)\Bigg|_{r=r_{\Omega}}. \tag{49}$$

The energy-dependent width is obtained directly from Eq. (15). For the Hilbert transform in Eq. (16) we use a simple trapezoidal-like integration rule based on the formula

$$\int_{x_1}^{x_2} \frac{ax+b}{x_0 - x} \mathrm{d}x = a(x_1 - x_2) + (ax_0 + b)\ln\left| \frac{x_1 - x_0}{x_2 - x_0} \right|. \tag{50}$$

(more sophisticated methods for performing the numerical Hilbert transform can be found in the Appendix of Ref. [16] and in Ref. [35], and references therein).

The generalization of the FFR procedure to the case of more than one resonance in the Σ_{res} domain is quite straightforward. For construction of the projector Q we need the discrete states to be orthogonal to each other, namely

$$\int_0^{r_{\Omega}} \varphi_{d,i}^*(r) \varphi_{d,j}(r) dr = 0, \quad i \neq j. \tag{51}$$

The orientation of the vectors is not uniquely determined; one of the good possibilities is to diagonalize the operator QHQ in the basis of the discrete states. Generally this choice slightly simplifies calculations [cf. Eq. (9)]. In the case of several separated resonances the off-diagonal terms of the operator $\epsilon - H_{QQ} - H_{QP}(\epsilon - H_{PP} + i\varepsilon)^{-1} H_{PQ}$ can be neglected and the resonant contribution to the phase shift is well approximated by the sum of Breit-Wigner terms. This shows that each discrete state corresponds to one resonance. We can

expect that such a definition leads to smoother discrete-state–continuum couplings. Moreover, it preserves the validity of the approximation (39).

D. Extensions of the FFR method

In this section we propose several variants of the FFR method, that are analyzed in Sec. III. The variants differ mainly in the way they treat the overlaps $\langle {}^{\circ}\varphi_j^{\Omega}|\varphi_k^{\Omega}\rangle$ in Eq. (29). In the *Nestmann approximation* method (NA) [20] the overlap integrals are evaluated using Eq. (39), but the coupling element $\langle {}^{\circ}\varphi_j^{\Omega}|H^{\Omega}|\varphi_d\rangle$ is assumed to be j-independent and therefore can be omitted in Eqs. (39) and (41). The coefficients B_k are then determined from Eq. (41) directly without any initial guess of the discrete state wave function and the iterative process (42)–(45) is avoided. The center of attention will be on the *improved Nestmann approximation* method (INA). In INA, the system (29) is solved using approximate overlaps defined by Eqs. (39)–(45).

A quite different approach is used in the *additional level method* (AL). In the AL method the system (29) is solved exactly within the Σ_{res} domain (possibly different than in the INA method) and the condition (24) is satisfied subsequently by adding the first level above Σ_{res} into the discrete state expansion with the proper coefficient. If the model system and the Σ_{res} domain are chosen properly, this addition represents just a small correction and the FFR idea is not violated. The major disadvantage of the AL method is that the overlap integrals have to be evaluated explicitly.

In addition we will refer also to the *orthogonalisation method* (OM). In this method the discrete state is determined simply by the solution of Eq. (29). This method produces a nonintegrable wave function $|\varphi_d\rangle$ which cannot be used rigorously in order to define the subspace $\mathcal{Q}$. Within this approach the T-matrix is equal to $T_{bg}+T_{res}$ approximatively only. However, it provides a very illustrative comparison with the other methods.

III. MODEL STUDIES

This section is devoted to the study of the performance of the methods discussed in the previous section. We have applied the FFR method to several spherically symmetric potential scattering problems and here we present some illustrative results, comparing different versions of FFR as listed in Sec. II D. Particular attention is paid to the dependence of z_{res}, $\Gamma(\epsilon)$, and δ_{bg} on (unphysical) quantities like r_Ω, Σ_{res}, and ${}^{\circ}H$ for each method. Throughout the whole section we use atomic units and reduced mass $\mu=1$.

A. Square well with centrifugal barrier (potential A)

The square well with centrifugal barrier is a typical potential supporting resonances in atomic and molecular physics: a combination of an attractive short-range potential and the repulsive centrifugal barrier for $J\neq 0$. With parameters set to $a=3$, $B=2$, and $J=4$ the potential

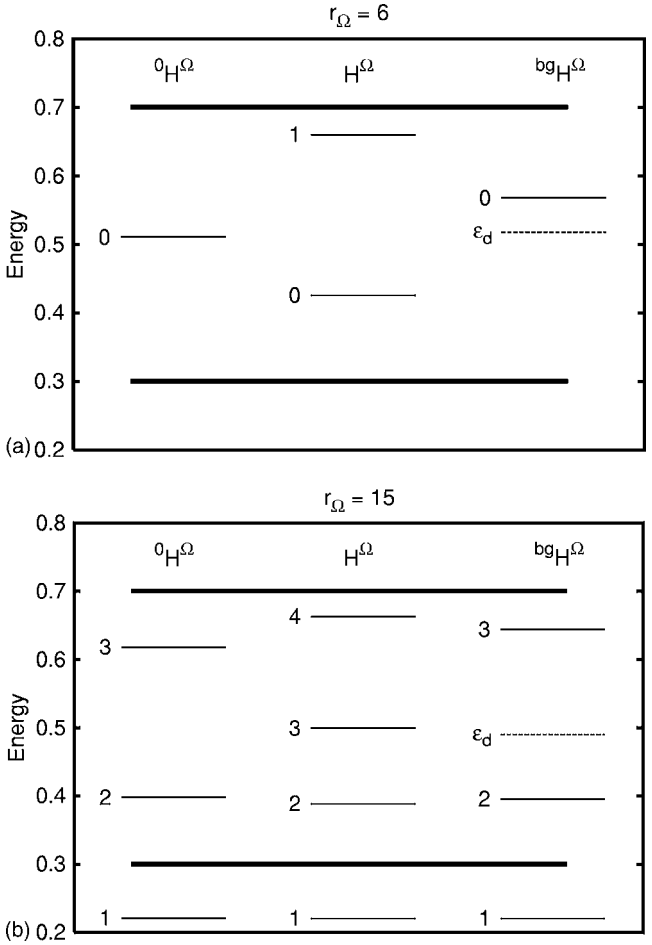

FIG. 2. Potential A: R-matrix spectra for two values of the R-matrix radius. From left: model potential spectrum, original potential spectrum, and the separated spectrum; solid lines: background spectrum; dashed line: discrete state position determined by the INA method. Thick lines demarcate the Σ_{res} domain.

$$V_A(r)=\begin{cases}\dfrac{J(J+1)}{2r^2}-B & r<a\\ \dfrac{J(J+1)}{2r^2} & r\geqslant a\end{cases} \tag{52}$$

possesses an isolated resonance at the energy $z_{res}=0.488-0.036i$. As a model system we use the potential of the corresponding centrifugal barrier

$${}^{\circ}V_A(r)=\frac{J_0(J_0+1)}{2r^2},\quad J_0=J. \tag{53}$$

The R-matrix spectra for the full and model potentials for two values of the R-matrix radius r_Ω are plotted in Fig. 2. Background phase shifts δ_{bg} separated by different methods are plotted in Fig. 3, the discrete state wave functions and corresponding resonance width functions are shown in Figs. 4 and 5.

In the case $r_\Omega=6$, $\Sigma_{res}=\langle 0.3,0.7\rangle$ contains only two spectral levels of the full problem ($N=2$, ${}^{\circ}N=1$) and the discrete state is completely determined by Eq. (24). In such a case all

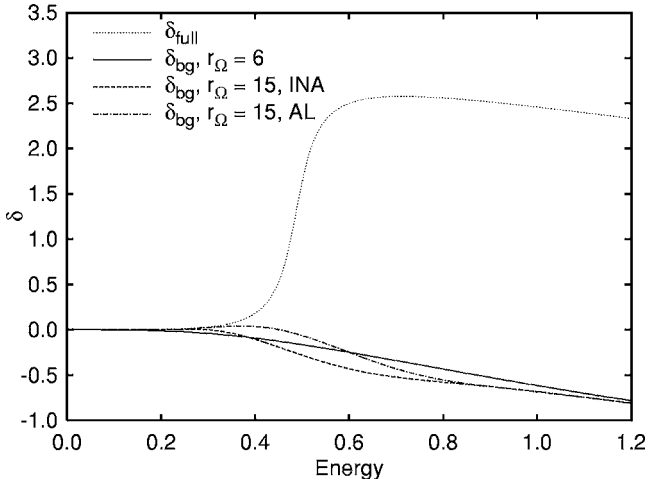

FIG. 3. Potential A: Full phase shift and background phase shifts obtained with different versions of FFR and different dimensions of the R-matrix sphere.

versions (except OM) of the FFR methods are equivalent. With increasing r_Ω the R-matrix spectrum becomes more dense, for $r_\Omega=15$, $N=3$, and $^\circ N=2$. The smoothest background phase shift is produced with $r_\Omega=6$ but, also for $r_\Omega=15$, the resonance is well separated out using both the INA and AL methods. Nevertheless, there is a qualitative difference between the discrete state wave functions. For $r_\Omega=6$ the wave function $\varphi_d(r)$ shows no oscillations. It looks like a typical bound-state wave function. With increasing r_Ω $\varphi_d(r)$ oscillates for $r \geqslant 6$. In the OM method the amplitude of the oscillations is constant and the frequency does not correspond to the energy of the discrete state $\epsilon_d^{\mathrm{OM}}=0.5459$ but rather to an energy lying slightly above Σ_{res}. In both the INA and AL methods the oscillations are damped and the wave functions vanish at r_Ω. The frequency of the oscillations is lowered and corresponds approximately to the discrete state energy ϵ_d. In the AL method the discrete state lies above the resonance energy ϵ_{res} at $\epsilon_d^{\mathrm{AL}}=0.5116$, the wave function follows closely $\varphi_d^{\mathrm{OM}}(r)$ in the interaction region. In the INA

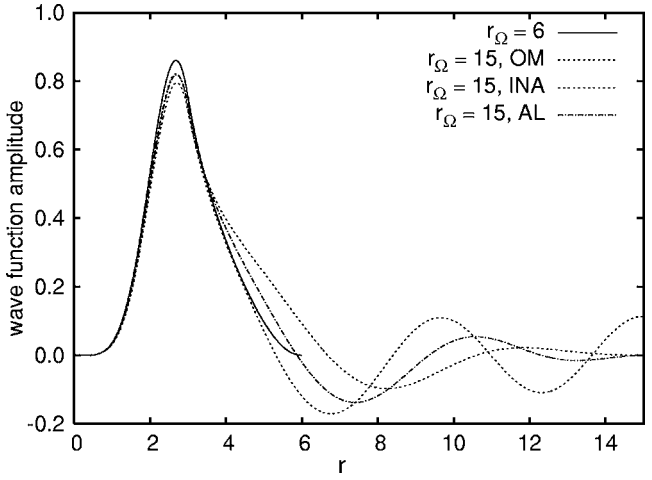

FIG. 4. Potential A: discrete state wave functions obtained with different versions of FFR and different dimensions of the R-matrix sphere.

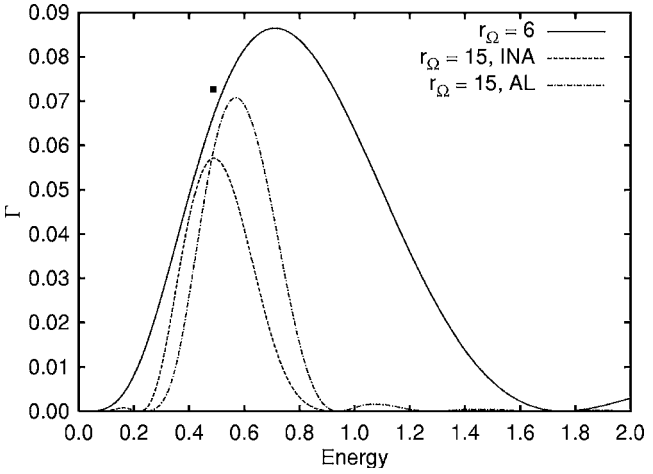

FIG. 5. Potential A: energy dependent resonance width functions corresponding to different discrete states, cf. Fig. 4. The black square shows the local (Siegert) resonance position and width.

method the discrete state energy $\epsilon_d^{\mathrm{INA}}=0.4898$ is almost equal to the resonance position ϵ_{res} and the oscillations are very quickly damped.

In general, we observe that $\varphi_d(r)$ does not oscillate if we choose r_Ω within the interval $\langle r_{\mathrm{int}}, r_{\mathrm{int}}+\lambda_{\epsilon_d}\rangle$, where r_{int} is the "interaction range" and λ_{ϵ_d} the de Broglie wavelength associated to ϵ_d. The interaction range r_{int} is defined here as the region where the amplitude of the scattering wave function at the resonance energy is enhanced.

Although the background phase shifts are quite similar in all cases (Fig. 3), the resonance energy-dependent widths are very different from each other, see Fig. 5. However, the local (Siegert) resonance energy and widths (positions of the corresponding S-matrix poles in complex energy plane, $z_{res}=\epsilon_{res}-i\Gamma_{res}/2$) obtained from Eq. (1) are the same for all three cases, $z_{res}=0.488-0.036i$, differing only at the level of the error of the rational interpolation used to extend $F(\epsilon)$ to the complex energy plane. Therefore all the methods are equivalent from this point of view. However, the suitability of each method may differ depending on particular application of the FFR method.

To investigate the sensitivity of the method to the model potential we have performed the separation with different values of J_0 in Eq. (53). Resulting background phase shifts δ_{bg} are plotted in Fig. 6. We have used also the unphysical noninteger values of J_0 to obtain smoother dependence. From Fig. 6 we observe that in the case of INA and AL methods all values of J_0 from 3 to 6 result in a weakly energy-dependent background phase shift, i.e., in a satisfactory resonance-background partitioning. On the other hand, the OM method provides weakly energy-dependent δ_{bg} only for $J_0=4$ or $J_0=5$. We can conclude that compared to the OM both the INA and AL procedures reduce the influence of the model potential V_0. Proper choice of the model potential is, however, very important. In general, the model potential should repel the wave functions $^\circ\varphi_j^\Omega(r)$ out of the interaction region so that the wave function $\varphi_d(r)$, which is orthogonal to $^\circ\varphi_j^\Omega(r)$, is localized in the interaction region.

Comparison of the discrete state wave functions determined by INA and AL methods for $J_0=4$ and $J_0=5$ is pre-

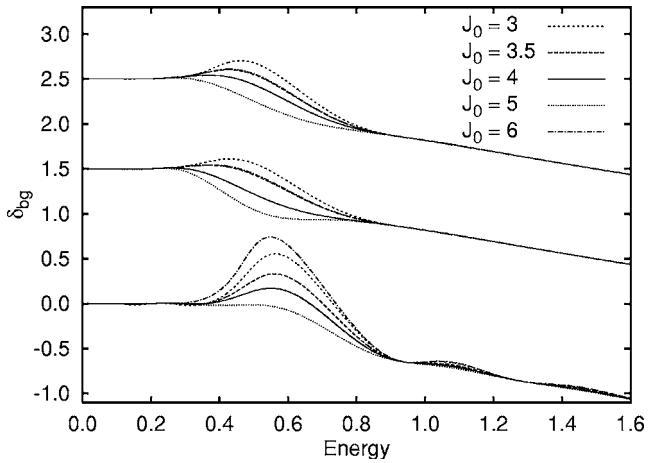

FIG. 6. Potential A: background phase shifts obtained by the FFR method with different model potentials. Lowest curves were obtained by OM, results of INA are shifted by 1.5, and results of AL by 2.5.

sented in Fig. 7. It is interesting to note that the discrete state wave function separated by INA with $J_0=4$ is almost exactly equal to $\varphi_d{}^{\mathrm{AL}}(r)$ determined with $J_0=5$. Equivalence of the INA and AL methods with different J_0 shows that the application of the Nestmann approximation is equivalent to a slight modification of the model potential. In the case above the Nestmann approximation yields values of overlap integrals $\langle {}^{\circ}\varphi_j^{\Omega}|\varphi_k^{\Omega}\rangle$ for $J_0=4$ that are closer to $\langle {}^{\circ}\varphi_j^{\Omega}|\varphi_k^{\Omega}\rangle$ for $J_0=5$ than to their exact values.

B. Short-range potential (potential B)

In this section we discuss a smooth potential without centrifugal barrier, which serves as a standard test and which has been studied by various methods in the past [36–39].

The potential

$$V_B(r) = \frac{\lambda}{2} r^2 e^{-r} \tag{54}$$

can support resonances of a large range of widths, depending on the value of the parameter λ. The resonance poles are

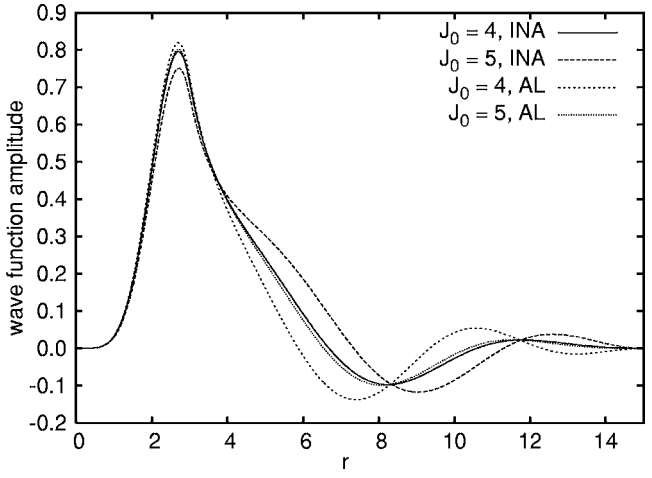

FIG. 7. Potential A: Discrete state wave functions determined by the INA and AL methods with two different model potentials.

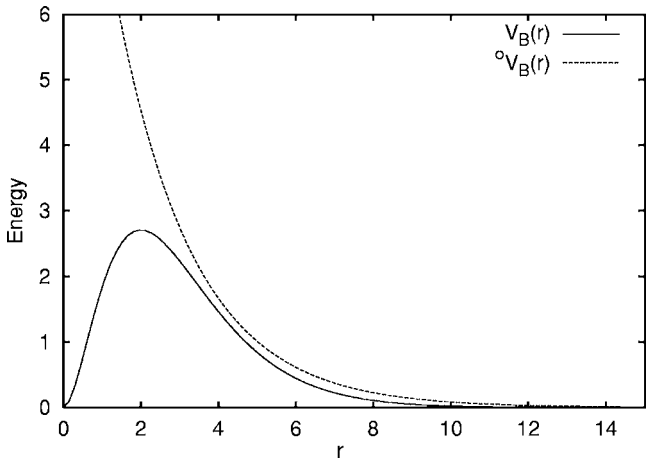

FIG. 8. Potential $V_B(r)$ with model potential ${}^{\circ}V_B(r)$, $\lambda=10$, $\lambda_0=11$.

determined in Ref. [8] for λ from 3 to 26 using two different methods of the shooting type based on the calculation of the Siegert state. We have applied the NA, INA, and AL methods to this potential in order to compute the resonance positions and widths. As a model system we have used the potential

$$^{\circ}V_B(r) = \frac{\lambda_0}{4} e^{-(r-3)/2} \tag{55}$$

with $\lambda_0=\lambda+1$; see Fig. 8.

Results obtained by the INA method are compared with accurate values from Ref. [8] in Table I. Trajectory of the resonance pole for λ from 3 to 26 is plotted in Fig. 9. For $\lambda>7$ where the resonance becomes narrow with $\Gamma_{res}<0.20$ our results correspond to Ref. [8] precisely. In order to obtain the positions of the resonance poles in the lower complex energy plane the level shift function $F(\epsilon)$ [Eq. (12)] is analytically continued to complex ϵ via rational extrapolation. The error bars in Fig. 9 are estimated from the dependence of the calculated resonance position on the set of points (on the real axis) used to construct the rational function. For more details see the Bulirsch-Stoer algorithm [40]. In Table I we list results of only one version of the FFR method, because for $\lambda>5$ all three studied variants yield results identical to at least three digits, which is comparable with the accuracy of the extrapolation. With increasing λ the accuracy improves as $\Gamma(\epsilon)$ becomes smoother for narrower resonances. For $\lambda \leqslant 5$ the results of different versions of FFR vary (see Fig. 9), but we have not observed any systematic trend in the deviations.

We observe that, although all three methods determine the positions of the resonance poles comparably well, the sensitivity of the methods to the size of the Σ_{res} domain is very diverse. The results of the AL method are rather independent on the definition of Σ_{res}. In the INA method the results are quite stable in a narrow range around the optimal definition of Σ_{res} [yielding the smoothest δ_{bg} and $\Gamma(\epsilon)$], i.e., if one or two more R-matrix levels $\varphi_k^{\Omega}(r)$ are added into the expansion of $\varphi_d(r)$, see Eq. (23). For the NA method there is usually only one suitable choice of Σ_{res}, any other definition leads to

TABLE I. Potential B: resonance energies and local widths obtained by the INA version of the FFR method and by the shooting method (SM) [8]. Stars indicate where the discrete state is expanded into only two levels in the NA method; see text. Numbers in square brackets denote powers of 10.

λ	$\epsilon_{res}^{\mathrm{INA}}$	$\Gamma_{res}^{\mathrm{INA}}/2$	$\epsilon_{res}^{\mathrm{SM}}$	$\Gamma_{res}^{\mathrm{SM}}/2$
3*	1.0969	2.1180[−1]	9.7382[−1]	2.1541[−1]
4	1.2318	1.6496[−1]	1.2342	1.8723[−1]
5*	1.4797	1.5322[−1]	1.4779	1.5912[−1]
6*	1.7202	1.3730[−1]	1.7089	1.3279[−1]
7*	1.9232	1.0993[−1]	1.9294	1.0900[−1]
8	2.1407	8.9535[−2]	2.1409	8.8039[−2]
9*	2.3448	7.0063[−2]	2.3443	6.9980[−2]
10*	2.5411	5.4772[−2]	2.5405	5.4741[−2]
11	2.7302	4.2179[−2]	2.7298	4.2144[−2]
12	2.9121	3.1832[−2]	2.9127	3.1944[−2]
13	3.0900	2.3813[−2]	3.0895	2.3854[−2]
14	3.2612	1.7562[−2]	3.2607	1.7567[−2]
15*	3.4263	1.2762[−2]	3.4264	1.2774[−2]
16*	3.5866	9.2165[−3]	3.5870	9.1865[−3]
17	3.7425	6.5474[−3]	3.7429	6.5436[−3]
18	3.8946	4.6205[−3]	3.8944	4.6243[−3]
19	4.0418	3.2468[−3]	4.0418	3.2472[−3]
20	4.1856	2.2661[−3]	4.1853	2.2688[−3]
21*	4.3251	1.5790[−3]	4.3254	1.5794[−3]
22	4.4621	1.0977[−3]	4.4621	1.0965[−3]
23	4.5956	7.5891[−4]	4.5959	7.5988[−4]
24	4.7270	5.2596[−4]	4.7268	5.2606[−4]
25	4.8551	3.6409[−4]	4.8550	3.6402[−4]
26	4.9811	2.5167[−4]	4.9808	2.5191[−4]

a very strong dependence of $\Gamma^{\mathrm{NA}}(\epsilon)$ on the energy. Furthermore, for some values of λ (denoted by stars in Table I) it appears that the discrete state has to be represented by two levels $\varphi_k^{\Omega}(r)$ only to obtain smooth $\Gamma(\epsilon)$.

Figures 10–12 demonstrate the advantages of the INA over the NA method on the example of the potential B with $\lambda=10$. We compare two definitions of the Σ_{res} domain: the smaller one $\Sigma_{res}=\langle 2.1, 2.7\rangle$ with $N=2$, $^{\circ}N=1$, and the larger one $\Sigma_{res}=\langle 1.7, 3.5\rangle$ with $N=4$, $^{\circ}N=3$. Discrete state wave functions determined by the NA and INA methods are plotted in Fig. 10. The wave functions obtained with the smaller Σ_{res} [with $N=2$, both methods are reduced to Eq. (24) and therefore equivalent] and by the NA method with the larger Σ_{res} have nearly the same amplitude in the vicinity of $r=0$ and exhibit pronounced, slowly damped oscillations for larger r. In case of the smaller Σ_{res} the enhanced peak close to $r=0$ has a complicated structure as both levels $\varphi_k^{\Omega}(r)$ are included into the $\varphi_d(r)$ expansion with comparable coefficients. $\varphi_d(r)$ obtained by the INA method with the larger Σ_{res} resembles more closely the bound-state wave function, oscillations beyond $r=4$ have small amplitude and are very quickly damped.

From Fig. 11 we observe that with $N=2$ the resonance is separated from the full phase shift (i.e., δ_{bg} does not rapidly

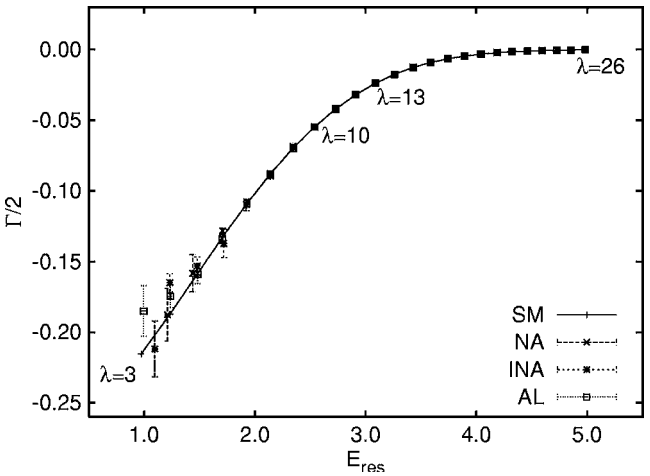

FIG. 9. Potential B: resonance pole trajectory for λ from 3 to 26. The error bars of the results of FFR methods were estimated from the stability of the rational interpolation of $F(\epsilon)$ in Eq. (1).

increase at the position of the resonance), but the background phase shift is not completely flat. The energy-dependent resonance width is bell shaped and attains its maximum to the left of the resonance position. It exhibits small oscillations at lower and higher energies (Fig. 12). Inclusion of the two more R-matrix levels (larger Σ_{res}) into the discrete state expansion results in a smoother energy dependence of δ_{bg} and $\Gamma(\epsilon)$ if the INA method is used. The background phase shift is flat and the energy-dependent resonance width is smaller, its maximum is located close to the resonance energy. On the other hand, the NA method yields much worse results. The energy-dependent resonance width has three peaks in the energy range (1.5, 3.6) and the background phase shift oscillates. The S-matrix pole, however, is determined correctly. These results show that in some cases the Nestmann approximation is too crude. In particular, neglecting the j-dependence of the couplings $\langle {}^{\circ}\varphi_j^{\Omega}|H^{\Omega}|\varphi_d\rangle$ in Eq. (39), which is related to the energy-independent discrete state-continuum coupling hypothesis, is not justified. Nevertheless, it should be stressed that the NA method can be used

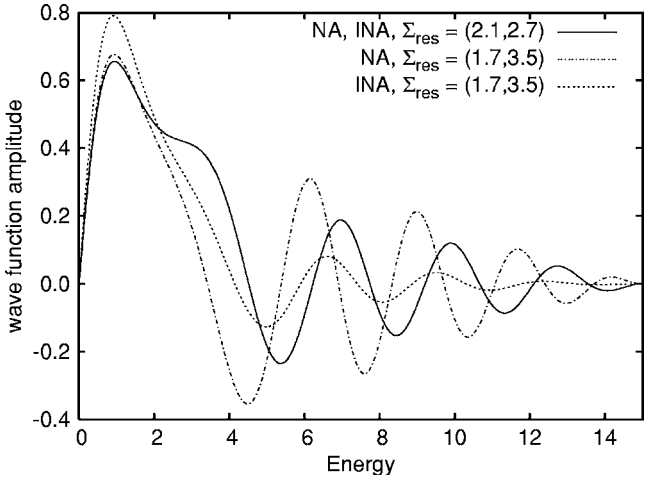

FIG. 10. Potential B, $\lambda=10$: discrete state wave functions defined by the NA and INA methods with different Σ_{res}.

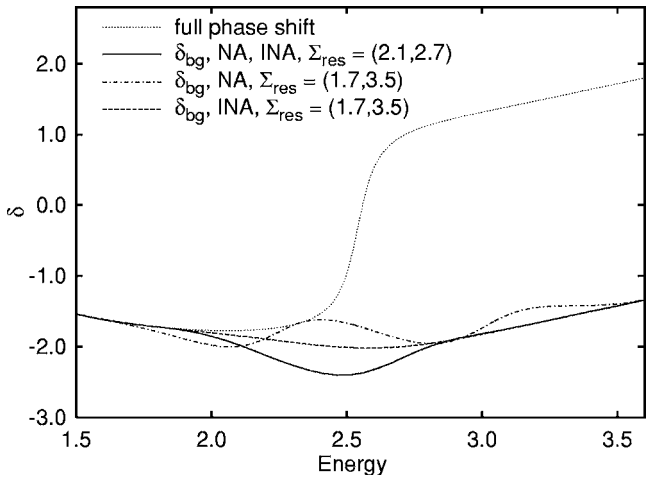

FIG. 11. Potential B, $\lambda=10$: background phase shifts separated by the NA and INA methods with different Σ_{res}.

in these cases provided the Σ_{res} domain, which contains only two R-matrix levels, is broad enough to allow for the full extraction of the resonance from the background scattering.

For narrower resonances (larger λ) NA works generally better, as shown Fig. 13, where the energy-dependent resonance width determined by all three variants of the FFR method is plotted. The same definition of $\Sigma_{res}=\langle 2.7, 3.6\rangle$ ($N=3$, $^{\circ}N=2$) is used in Fig. 13. However, it is not only the resonance width that determines the applicability of the Nestmann approximation. The approximation fails also for $\lambda=15$, 16, and 21. This failure is not caused by a wrong choice of the model potential; we found the NA results to be quite stable for a wide range of λ_0 in the model potential $^{\circ}V_B(r)$. The results can be, however, significantly improved by a change (even very small) of r_Ω. This underlines the sensitivity of the NA method to the choice of r_Ω.

IV. CONCLUSIONS

Though numerous methods are nowadays available for computing resonances, the FF method remains very appealing in particular for the following reasons: (i) this method focuses on physically relevant resonances only, and (ii) provides an interpretation of the resonances in terms of square integrable functions (the discrete states φ_d). Its major drawback is that it requires the *a priori* definition of the linear functional space $\mathcal{Q}$ in which the discrete states are expanded. This choice is usually evident in the case of Feshbach resonances but can be difficult in the case of shape resonances.

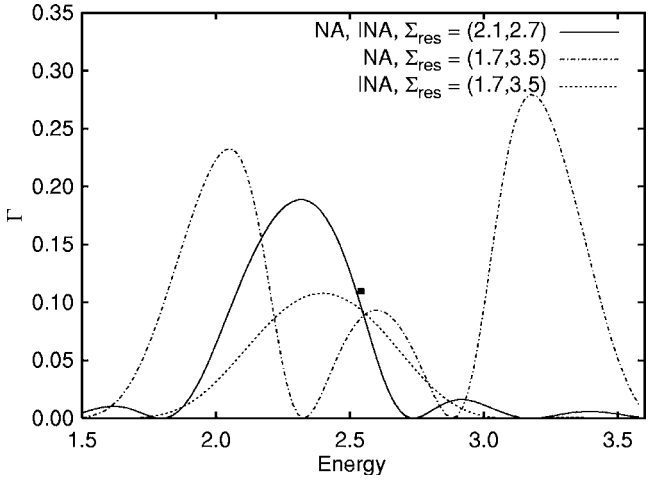

FIG. 12. Potential B, $\lambda=10$: resonance widths determined by the NA and INA methods with different Σ_{res}. The black square shows the local resonance position and width.

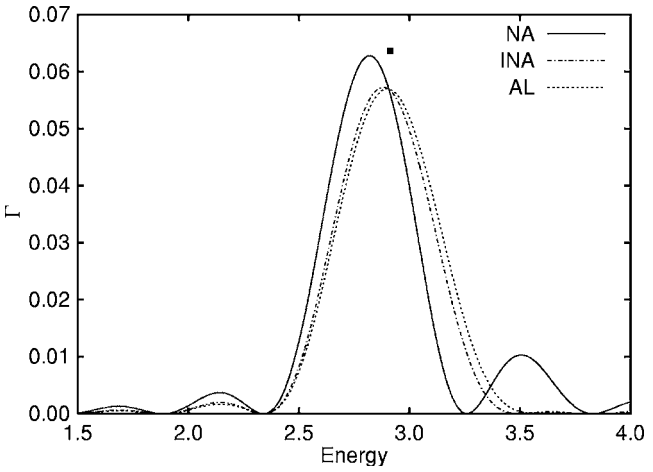

FIG. 13. Potential B, $\lambda=12$: resonance widths determined by different variants of the FFR method with the same $\Sigma_{res}=\langle 2.7, 3.6\rangle$ ($N=3$, $^{\circ}N=2$). The black square shows the local resonance position and width.

Nestmann has proposed a systematic approach for determining $\mathcal{Q}$ [20], the FFR method, which proved very powerful for computing cross sections of resonant electron-molecule collisions, in the case of shape [20,27–30] as well as Feshbach resonances [31,32]. The FFR method provides the discrete state, its potential curve, and the associated coupling terms to the background continuum. Within the FFR approach, the R-matrix spectrum E_l^{Ω} of the resonant system is compared within a given energy range Σ_{res} with the R-matrix spectrum $^{\circ}E_l^{\Omega}$ of a so-called model system similar to the studied one but exhibiting no resonance in Σ_{res}. The FFR method therefore requires *a priori* definition of both Σ_{res} and the model system.

The main limitation of the FFR method is that it can only be applied to systems which can be investigated via the R-matrix method. In the context of electron-molecule scattering, this constraint currently corresponds to low-energy scattering ($\leqslant$10 eV) and to small molecular systems ($\leqslant$40 electrons) (see, e.g., Refs. [27,41]). Nevertheless, technical improvements allowing consideration of a larger active space for the expansion of the scattering wave function may allow near future progress [42,43]. In the case of molecular collisions, the R-matrix theory can be applied to low-energy scattering involving not too heavy projectiles (see, e.g., Ref. [44]).

In this paper we have tested the FFR method on two qualitatively different spherically symmetric potential scattering problems—the square well with long-range centrifugal barrier and a smooth short-range potential. We compared three variants of the FFR method, the *Nestmann approximation, improved Nestmann approximation*, and *additional level*

methods. In all cases the FFR procedure resulted in a correct resonance-background partitioning, giving correct positions of the resonance poles in the complex energy plane. We found out that the influence of the model potential on the results is rather small, which is very important for practical applications where the possibilities of the choice of the model system are strongly limited. The major advantage of the NA and INA methods over the AL method is that once the poles E_k^Ω and ${}^\circ E_j^\Omega$ and the amplitudes $\varphi_k^\Omega(r_\Omega)$ and ${}^\circ\varphi_j^\Omega(r_\Omega)$ are known these algorithms are very easily programmed and not time consuming. The AL method, on the other hand, requires explicit knowledge of the overlap integrals $\langle {}^\circ\varphi_l^\Omega | \varphi_k^\Omega \rangle$, which are easily computed in case of one-dimensional systems but may get more difficult to obtain in realistic more-dimensional systems.

Our analysis also revealed some limitations of the method. We have shown that the NA method is very sensitive to the choice of the R-matrix radius r_Ω and the Σ_{res} domain. If r_Ω is chosen close to the "interaction range" r_{int} (the region where the amplitude of the scattering wave function at the resonance energy is enhanced) then the discrete state wave function $\varphi_d(r)$ looks like a typical bound-state wave function and the background phase shift and the resonance width depend weakly on energy. However, if r_Ω is larger the discrete state wave function oscillates for $r > r_{\text{int}}$, which may cause the resonance width to be strongly energy dependent. Both INA and AL methods proved to be significant upgrades of the NA method, giving better results [i.e., smoother energy-dependent quantities like $\Gamma(E)$ and δ_{bg}] less sensitive to the (unphysical) parameters r_Ω and Σ_{res}. The INA method is a rather slight modification of the NA method, preserving the advantage of numerically cheap indirect evaluation of the overlap integrals $\langle {}^\circ\varphi_l^\Omega | \varphi_k^\Omega \rangle$, and can therefore be easily implemented into existing R-matrix computer codes.

Though we have shown that all three methods provide correct resonance positions, their respective usefulness in the context of electron-molecule scattering must further be investigated. In order to obtain a correct diabatization of the metastable anionic state, not only the weak energy dependence of the discrete state background continuum coupling terms but also their smooth dependence on the molecular geometry is required. This feature, however, cannot be investigated in the context of spherically symmetric potential scattering and is still an open question. In all applications of the FFR procedure to electron-molecule scattering [20,27–32], the method yielded very good results. However, the de Broglie wavelength corresponding to the discrete state energy was in all studied systems comparable with the R-matrix radius ($r_\Omega = 10$ bohr), used in the calculations. We have shown that, in such a case, the results are quite independent on the particular level of approximation used in order to define $|\varphi_d\rangle$. This is due to the fact that all methods lead to a nonoscillating discrete state wave function and therefore to a smoothly energy-dependent resonance width function.

ACKNOWLEDGMENTS

The authors are thankful to B. M. Nestmann (Bonn) for his hospitality and useful discussions. This work was supported by the European Union via the Framework V Network "Electron and Positron Induced Chemistry" (EPIC) and the European Science Foundation (ESF) within the "Electron Induced Processes at the Molecular Level" (EIPAM) program.

[1] Y. V. Fyodorov and H. J. Sommers, J. Math. Phys. **38**, 1918 (1997).
[2] M. Desouter-Lecomte and X. Chapuisat, Phys. Chem. Chem. Phys. **1**, 2635 (1999).
[3] R. Santra and L. S. Cederbaum, Phys. Rep. **368**, 1 (2002).
[4] J. Ołowicz, M. Płoszajczak, and I. Rotter, Phys. Rep. **374**, 271 (2003).
[5] V. I. Kukulin, V. M. Krasnopolsky, and J. Horáček, *Theory of Resonances: Principles and Applications* (Kluwer Academic Publishers, Dordrecht, 1989).
[6] A. U. Hazi, J. Phys. B **11**, L259 (1978).
[7] V. A. Mandelshtam, T. R. Ravuri, and H. S. Taylor, J. Chem. Phys. **101**, 8792 (1994).
[8] M. Čížek and J. Horáček, J. Phys. A **29**, 6325 (1996).
[9] N. Moiseyev, Phys. Rep. **302**, 211 (1998).
[10] G. Breit and E. P. Wigner, Phys. Rev. **49**, 519 (1936).
[11] P. I. Kapur and R. Peierls, Proc. R. Soc. London, Ser. A **166**, 277(1938).
[12] E. P. Wigner and L. Eisenbud, Phys. Rev. **72**, 29 (1947).
[13] U. Fano, Phys. Rev. **124**, 1866 (1961).
[14] H. Feshbach, Ann. Phys. (N.Y.) **5**, 357 (1958).
[15] H. Feshbach, Ann. Phys. (N.Y.) **19**, 287 (1962).
[16] M. Desouter-Lecomte, J. Liévin, and V. Brems, J. Chem. Phys. **103**, 4524 (1995).
[17] V. Brems, M. Desouter-Lecomte, and J. Liévin, J. Chem. Phys. **104**, 2222 (1996).
[18] M. Desouter-Lecomte and J. Liévin, J. Chem. Phys. **107**, 1428 (1997).
[19] V. Brems and M. Desouter-Lecomte, J. Chem. Phys. **116**, 8318 (2002).
[20] B. M. Nestmann, J. Phys. B **31**, 3929 (1998).
[21] W. Domcke, Phys. Rep. **208**, 97 (1991).
[22] M. Allan, M. Čížek, J. Horáček, and W. Domcke, J. Phys. B **33**, L209 (2000).
[23] P. Kolorenč, M. Čížek, J. Horáček, G. Milnikov, and H. Nakamura, Phys. Scr. **65**, 328 (2002).
[24] T. Sommerfeld and H.-D. Meyer, J. Phys. B **35**, 1841 (2002).
[25] A. K. Kazansky, J. Phys. B **31**, L431 (1998).
[26] I. Rotter, Acta Phys. Pol. B **35**, 1269 (2004).
[27] T. Beyer, B. M. Nestmann, and S. D. Peyerimhoff, Chem. Phys. **255**, 1 (2000).
[28] T. Beyer, B. M. Nestmann, and S. D. Peyerimhoff, J. Phys. B **33**, 4657 (2000).
[29] T. Beyer, B. Nestmann, and S. Peyerimhoff, J. Phys. B **34**, 3703 (2001).
[30] V. Brems, T. Beyer, B. M. Nestmann, H.-D. Meyer, and L. S.

Cederbaum, J. Chem. Phys. **117**, 10635 (2002).
[31] B. M. Nestmann, S. V. K. Kumar, and S. D. Peyerimhoff, Phys. Rev. A **71**, 012705 (2005).
[32] B. M. Nestmann, V. Brems, A. K. Dora, and S. Kumar, J. Phys. B **38**, 75 (2005).
[33] W. Domcke, Phys. Rev. A **28**, 2777 (1983).
[34] P. G. Burke and K. A. Berrington, *Atomic and Molecular Processes: An R-Matrix Approach* (IOP Publishing, Bristol, 1993).
[35] M. Polášek, M. Juřek, M. Ingr, P. Čársky, and J. Horáček, Phys. Rev. A **61**, 032701 (2000).
[36] R. A. Bain, J. N. Bardsley, B. R. Junker, and C. V. Sukumar, J. Phys. B **7**, 2189 (1974).
[37] H. D. Meyer and O. Walter, J. Phys. B **15**, 3647 (1982).
[38] F. M. Fernandez, J. Phys. A **28**, 4043 (1995).
[39] H. J. Korsch, H. Laurent, and R. Möhlenkaupf, Mol. Phys. **43**, 1441 (1981).
[40] J. Stoer and R. Bulirsh, *Introduction to Numerical Analysis* (Springer-Verlag, 1980).
[41] I. Rozum, N. Mason, and J. Tennyson, New J. Phys. **5**, 155.1(2003).
[42] K. Pfingst, B. M. Nestmann, and S. D. Peyerimhoff, J. Phys. B **27**, 27 (1994).
[43] J. Tennyson, J. Phys. B **37**, 1061 (2004).
[44] D. Lauvergnat and D. C. Clary, J. Chem. Phys. **108**, 3566 (1998).